Magnetochromic effect in multiferroic RIn_{1−x}Mn_{x}O_{3} (R=Tb, Dy)

P. Chen, B. S. Holinsworth, K. R. O'Neal, T. V. Brinzari, D. Mazumdar, C. V. Topping, X. Luo,

S.-W. Cheong, J. Singleton, S. McGill, and J. L. Musfeldt

Magnetochromic effect in multiferroic RIn$_{1-x}$Mn$_x$O$_3$ (R=Tb, Dy)

P. Chen,[1] B. S. Holinsworth,[1] K. R. O'Neal,[1] T. V. Brinzari,[1] D. Mazumdar,[1] C. V. Topping,[2] X. Luo,[3,4] S. -W. Cheong,[3,4] J. Singleton,[2] S. McGill,[5] and J. L. Musfeldt[1]

[1]*Department of Chemistry, University of Tennessee, Knoxville, Tennessee 37996, USA*
[2]*National High Magnetic Field Laboratory, Los Alamos National Laboratory, Los Alamos, New Mexico 87545, USA*
[3]*Rutgers Center for Emergent Materials and Department of Physics & Astronomy,*
Rutgers University, Piscataway, New Jersey 08854, USA
[4]*Laboratory for Pohang Emergent Materials and Department of Physics,*
Pohang University of Science and Technology, Pohang 790-784, Korea
[5]*National High Magnetic Field Laboratory, Tallahassee, Florida 32310, USA*
(Dated: March 10, 2015)

We combined high field magnetization and magneto-optical spectroscopy to investigate spin-charge coupling in Mn-substituted rare-earth indium oxides of chemical formula RIn$_{1-x}$Mn$_x$O$_3$ (R = Tb, Dy). The edge states, on-site Mn^{3+} d to d excitations, and rare-earth f-manifold excitations all track the magnetization energy due to dominant Zeeman interactions. The field-induced modifications to the rare-earth excitations are quite large because spin-orbit coupling naturally mixes spin and charge, suggesting that the next logical step in the design strategy should be to bring spin-orbit coupling onto the trigonal bipyramidal chromophore site with a 4 or 5d center.

I. INTRODUCTION

Spin-charge interactions are at the heart of the rich properties and tunability in complex oxides.[1–4] These processes are traditionally investigated by resistivity, polarization, and dielectric constant measurements in the presence of external stimuli like temperature, magnetic field, or pressure.[5–9] The frequency dependent parts of these response functions also reveal important signatures of magnetoelectric coupling. In fact, one of the remarkable findings from this class of work is how far beyond the static limit spin-charge interactions extend.[10] The temperature, pressure, and the field-induced band gap shifts in ZnO, BiFeO$_3$, and Ni$_3$V$_2$O$_8$ are but a few examples.[11–13] The visible color contrast in the latter can even be seen with the naked eye. Substituted rare-earth indium oxides attracted our attention as systems in which to amplify these interactions. In addition to ferroelectricity and magnetic frustration,[7,8,14,15] RIn$_{1-x}$Mn$_x$O$_3$ sports enormous spin-orbit coupling due to rare-earth incorporation (on the order of 2000 cm^{-1} for Tb^{3+} and Dy^{3+})[16] and the presence of a magnetic chromophore (in this case, Mn^{3+}).[17,18] The combination provides an opportunity to test how these factors influence the dynamic aspects of magnetoelectric coupling.

Rare-earth indium oxides crystallize in hexagonal structures (space group $P6_3cm$) and are isostructural with LuMnO$_3$.[19] The noncentrosymmetric structure gives rise to ferroelectricity in RInO$_3$.[17,18] Rare-earth centers form triangular lattices in the ab plane and result in frustration.[20] In the lattice structure, the In^{3+} ions are located in fivefold-coordinated trigonal-bipyramidal sites, and rare-earth ions are seven-fold coordinated with two different site symmetries C_3 and C_{3v}. When substituted with Mn^{3+}, the color changes dramatically, from white to rich blues and greens.[18] This is because Mn d-d excitations appear in the visible range. In magnetic field, these on-site excitations red shift due to the Zeeman effect.[21] In the more well-studied RMnO$_3$ systems, applied field reveals rich phase diagrams, an indication of the many nearly-degenerate states in these systems.[14] Rare-earth centers also introduce spin-orbit coupling and f-manifold excitations into the spectrum.[22] The magnetic field-induced shift of these excitations may provide an additional mechanism by which color properties can change.

One of the long term aims of our research program is to make materials that give large color changes with very small perturbation by magnetic field. In this work, we report dynamic magnetoelectric coupling in the RIn$_{1-x}$Mn$_x$O$_3$ (R = Tb, Dy) family of materials. Our measurements reveal broad, modestly-sized magneto-optical contrast due to edge states and on-site Mn^{3+} d to d excitations as well as dramatic but narrow field-induced changes in the f-manifold excitations of the rare-earth centers. Bringing these data together with complementary high-field magnetization reveals the key role of Zeeman splitting in each case. Short range correlations also enable these effects to persist to a surprisingly high temperature. These data suggest that the next logical step in the design strategy of color change materials should be to bring spin-orbit coupling onto the chromophore site (for instance with a 4 or 5d center). This modification should amplify the spin-charge interaction and yield larger field-induced color changes. Continued work in this direction will advance the understanding of spin-charge coupling away from the static limit.

II. METHODS

A series of polycrystalline RIn$_{1-x}$Mn$_x$O$_3$ (R= Tb, Dy) ceramics with x=0.003, 0.01, and 0.02 were prepared via conventional solid-state reactions.[18] Isothermal magnetization was measured using a 65 T short-pulse magnet

located at the National High Magnetic Field Laboratory at Los Alamos using the induction method and a coaxial compensation coil.[23] These results were benchmarked with low field measurements on a SQUID between 1.8 and 30 K with a 7 T field. Variable temperature and magneto-optical measurements were carried out at the National High Magnetic Field Laboratory at Tallahassee using a McPherson 2061A monochromator and a 35 T resistive magnet. Some transmittance runs were also performed using the 45 T hybrid magnet. Absorption was calculated as $\alpha(\omega) = \frac{-1}{d}\ln(T(\omega))$, where $T(\omega)$ is the transmittance as a function of photon frequency ω, and d is the sample thickness. Normalized absorption difference spectra were also calculated as $[\frac{\Delta\alpha(B)}{\alpha(0\ T)} = \frac{\alpha(35\ T) - \alpha(0\ T)}{\alpha(0\ T)}]$. Traditional peak fitting methods were employed as appropriate.

III. RESULTS AND DISCUSSION

III.1. Magnetization Overview

Figure 1(a) displays the isothermal magnetization of TbInO$_3$, DyInO$_3$, and two representative Mn-substituted systems as a function of magnetic field. The moments grow rapidly below 10 T, above which, the slopes decrease, and the moment changes quasi-linearly. At 65 T, the moments of TbInO$_3$ and DyInO$_3$ are $\approx$6.9 μ_B/Tb^{3+} and 8.1 μ_B/Dy^{3+}, respectively. These values are not fully saturated, although they are approaching the free ion magnetic moments of Tb^{3+} (9 μ_B) and Dy^{3+} (10.6 μ_B). The dM/dB curve of DyInO$_3$ also displays an 0.8 T local maximum. This finding along with low temperature ac susceptibility measurements (reported elsewhere) suggest that the structure is a spin glass transition.[24] Mn substitution introduces isolated paramagnetic impurities in the lattice. These materials have slightly higher saturation magnetizations compared with their unsubstituted analogs. Finally, Fig. 1(b) shows the temperature dependent magnetization of TbInO$_3$. Increasing temperature reduces the magnetization, although even well above the $\approx$0.16 K ordering temperature,[24] short range interactions preserve the characteristic shape of the curve. That a remnant of magnetic order in TbInO$_3$ appears at temperatures that are more than an order of magnitude above the long range ordering transition is not unique. Similar effects are observed in DyInO$_3$ and the Mn-substituted rare earth indium oxides. Analogous behavior occurs in other multiferroics and a number of molecule-based materials including [CuF$_2$(pyz)](H$_2$O)$_2$ and [CuHF$_2$(pyz)$_2$]BF$_4$.[23,25]

III.2. Optical properties of TbIn$_{1-x}$Mn$_x$O$_3$

Figure 2(a) displays the optical response of TbInO$_3$. We assign the rising absorption near 20000 cm^{-1} as part of the O 2p to In 5s charge transfer excitation.[26] An 18,000 cm^{-1} (2.2 eV) direct band gap is extracted from a
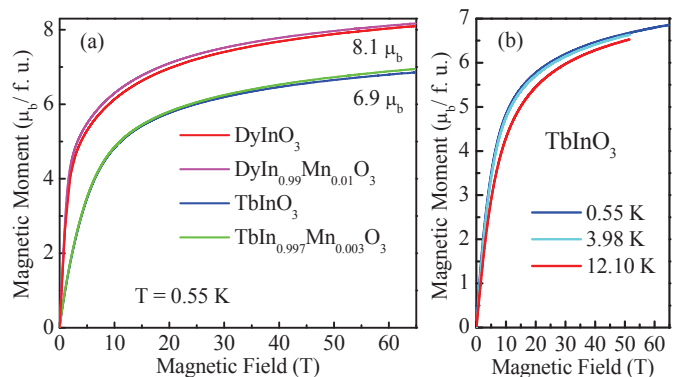

FIG. 1. (Color online) (a) Isothermal magnetization of DyInO$_3$, DyIn$_{0.99}$Mn$_{0.01}$O$_3$, TbInO$_3$, and TbIn$_{0.997}$Mn$_{0.003}$O$_3$ as a function of field at 0.55 K. (b) Temperature dependent magnetization of TbInO$_3$. As evidenced by the shape of the 12 K magnetization curve compared with that at 0.55 K, short range spin correlations are quite strong, even well above the ordering temperature.

linear fit of $(\alpha \cdot \omega)^2$ vs. ω, where α is the absorption coefficient and ω is the photon frequency.[27,28] With increasing magnetic field, absorption in the tail of the charge transfer excitation increases, probably due to changes in edge states. The normalized field-induced absorption difference spectrum of TbInO$_3$ is shown in the inset of Fig. 2(a). It displays a broad change with a maximum of 7% at 45 T near 14000 cm^{-1}. Absorption of more photons in the red-yellow color range makes the material appear less orange in high field. We can understand this effect in terms of change-spin coupling. As the system is driven toward the fully polarized state, the microscopic spin structure and moment are modified and, in the presence of strong spin-charge interactions, the electronic structure is modified as well.[13,29]

We quantify the field-induced color change with the integrated intensity $I(B) = \int_{\omega_1}^{\omega_2} \Delta\alpha(\omega, B)d\omega$, where ω_1 and ω_2 are the frequencies of integration. This quantity represents the change in absorption in magnetic field. Overall, $I(B)$ increases with field, and the change decreases at higher temperatures due to thermal effects [Fig. 2(b)]. This is because the system is harder to polarize at higher temperature. The trend is well described by the magnetization energy $C \int M(B)dB$, where $M(B)$ is the experimental magnetization (from Fig. 1) and C is a constant. This finding indicates that Zeeman energy is the driving force for the field-induced color change.[30]

Chemical substitution is an powerful strategy for tailoring magnetic and color properties.[31,32] When Mn^{3+} is substituted into the TbInO$_3$ matrix, paramagnetic spins are added, and magnetization increases slightly [Fig. 1]. At the same time, the color goes from golden-orange to green. This is because the Mn^{3+} d-d excitations appear in the visible range [Fig. 2(c)]. The broad features centered at 15900 and 17200 cm^{-1} are assigned as Mn^{3+} on-site excitations from d$_{xy}$/d$_{x^2-y^2}$ and d$_{yz}$/d$_{zx}$
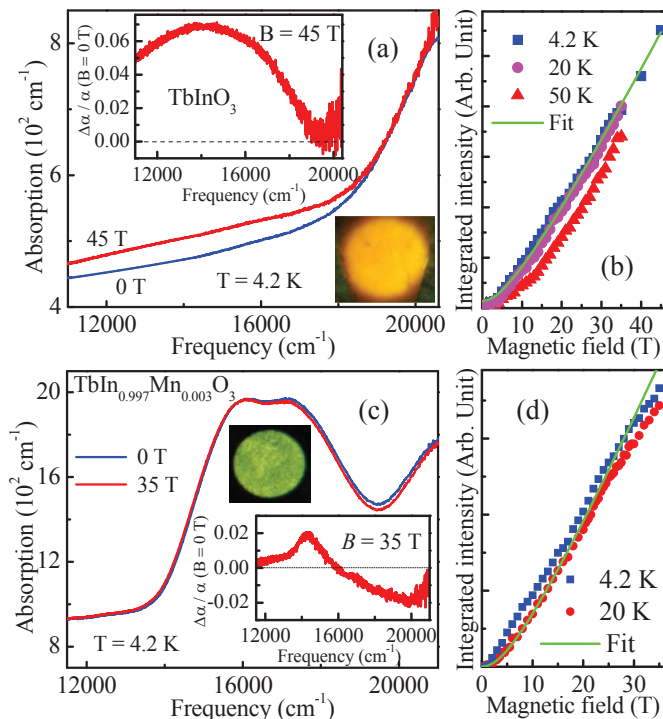
FIG. 2. (Color online) (a) Absorption coefficient, $\alpha(\omega)$, of TbInO$_3$ in 0 and 45 T at 4.2 K. Top inset: normalized absorption difference spectra $[\frac{\Delta\alpha(B)}{\alpha(0\ T)} = \frac{\alpha(45\ T) - \alpha(0\ T)}{\alpha(0\ T)}]$. Bottom inset: Photograph of a polished ≈ 100 μm sample in transmittance. (b) Integrated intensity in the range of excitation edge (12000 - 17000 cm^{-1}) as a function of magnetic field at selected temperatures: 4.2, 20 and 50 K. The integrated magnetization $C\int M(B)dB$ fits well with the integrated intensity trend, where $M(B)$ is the magnetization at $\sim$4 K and C is a constant. (c) Absorption coefficient of TbIn$_{0.997}$Mn$_{0.003}$O$_3$ in fields of 0 and 35 T at 4.2 K. Top inset: Photograph of a polished $\approx$33 μm sample in transmittance. Bottom inset: normalized absorption difference spectra. (d) Absolute value of the integrated intensity in the range of the excitation edge as a function of magnetic field at selected temperatures: 4.2 and 20 K.

to $d_{3z^2-r^2}$.[21,33] The inset of Fig. 2(c) displays the normalized field-induced absorption difference spectra. Two broad features with opposite signs are observed. They are attributed to the effect of field-induced shift of the d-d excitations to lower energy ($\approx$40 cm^{-1}). This result is consistent with prior high field work on TbMnO$_3$.[21] The shift in the Mn^{3+} on-site excitations can be quantified by the absolute value of the integrated intensity with magnetic field ($|I(B)|$). The color change is on the order of 2% at 35 T. Figure 2(d) shows that $|I(B)|$ increases with field. The overall shape of the 4.2 K data is somewhat less well fit by the magnetization energy than that in unsubstituted TbMnO$_3$. The slight deviations are probably due to local strains introduced by the different ion sizes (In vs. Mn) combined with spin disorder introduced by the paramagnetic ions. The field-induced shift is reduced at higher temperatures due to thermal effects.

III.3. Optical properties of DyIn$_{1-x}$Mn$_x$O$_3$

The optical and magnetic properties of DyInO$_3$ arise from 4f electrons in the Dy^{3+} centers and their interactions. Figure 3(a) displays the magneto-optical response of DyInO$_3$. The overall absorption in the visible range is low, consistent with the white color of the material. A great deal of fine structure is observed. These features are well known Dy^{3+} crystal field transitions from the ^{6}H$_{15/2}$ ground state to various excited states, as indicated.[34] With applied magnetic field, the 4f excitations shift to higher energy [inset, Fig. 3(a)]. This trend is especially strong below 20,000 cm^{-1} where a typical shift in 35 T is 100 cm^{-1}. By contrast, the features above 20000 cm^{-1} are relatively rigid. This is because they are formally spin-forbidden but become allowed due to spin-orbit coupling.[16] Their sensitivity to applied field is diminished as a result.

Figure 3(b) shows a close up view of selected f-manifold excitations. We assign the two multiplet clusters as ^{6}H$_{15/2}\rightarrow$ ^{6}F$_{3/2}$ and ^{6}H$_{15/2}\rightarrow$ ^{6}F$_{1/2}$ excitations, respectively.[34] The site group controls the symmetry properties of crystal field excitation levels. In DyInO$_3$, two different Dy^{3+} centers occupy positions with C$_{3v}$ and C$_3$ site symmetry, respectively.[35] The slightly different crystal fields at these two sites causes each level to split into a doublet. Group theory also predicts that the ^{6}F$_{3/2}$ level is further split into two components due to spin-orbit coupling and the trigonal symmetry around the Dy^{3+} centers.[35] Therefore, a symmetry analysis predicts a total four lines in the ^{6}H$_{15/2}\rightarrow$ ^{6}F$_{3/2}$ cluster and two in ^{6}H$_{15/2}\rightarrow$ ^{6}F$_{1/2}$ cluster, in excellent agreement with our spectroscopic results [Fig. 3(b)]. Color contrast in the vicinity of the symmetry-allowed f-manifold excitations is very large, on the order of 20 - 40 %, depending on the feature of interest.

The Zeeman effect is an incisive probe of the crystal field environment. As summarized in Fig. 3(b,c), the f-manifold excitations in DyInO$_3$ shift to higher energy with increasing field. This is due to a combination of Zeeman effects in the ground and excited states. At the same time, the intensity of C$_3$ site-related features decreases. Overall, the peak positions shift with field as the magnetization energy, $C\int M(B)dB + \gamma$, where $M(B)$ is the magnetization data, C is a fitting constant, and γ is the zero field splitting energy. The agreement is a well-known signature of Zeeman interactions.[30] Here, the γ's are larger for the ^{6}H$_{15/2}\rightarrow$ ^{6}F$_{1/2}$ excitation compared to the ^{6}H$_{15/2}\rightarrow$ ^{6}F$_{3/2}$ excitation due to the smaller M$_J$ quantum number in the ^{6}F$_{1/2}$ level.[36]

A consistency check of this analysis is useful. Assuming that Zeeman splitting in the excited states is negligible, we can obtain the frequency shift of these excitations by a simplified Brillouin function analysis:[30]

$$\Delta\omega = \frac{\mu B}{\hbar}\tanh(\frac{\mu B}{k_B T}). \tag{1}$$

FIG. 3. (Color online) (a) Absorption coefficient, $\alpha(\omega)$, of $DyInO_3$ in 0 and 35 T fields at 4.2 K. Top inset: Normalized absorption difference spectra $[\frac{\Delta\alpha(B)}{\alpha(0\ T)} = \frac{\alpha(35\ T) - \alpha(0\ T)}{\alpha(0\ T)}]$. Bottom inset: Photograph of a polished $\approx 300\ \mu m$ sample in transmittance. (b) Close-up view of selected f electron excitations $^6H_{15/2} \to\ ^6F_{3/2}$ and $^6H_{15/2} \to\ ^6F_{1/2}$ at different fields. (c) Peak position vs. magnetic field for these f manifold excitations. The red lines are a fit using $C \int M(B)dB + \gamma$, where $M(B)$ is the experimental magnetization, C is a constant, and γ is the zero field energy of the excitation. The green line shows the result of a Brillouin function analysis. (d) Absorption coefficient of $DyIn_{0.99}Mn_{0.01}O_3$ in fields of 0 and 35 T at 4.2 K. The f electron excitations are from ground state $^6H_{15/2}$ to excited states $^6F_{7/2}$, $^6F_{5/2}$, and $^6F_{3/2}$. Top inset: Normalized absorption difference spectra. Bottom inset: Photograph of a polished $\approx 100\ \mu m$ sample viewed in transmittance. The blue color comes from the on-site excitations of the Mn centers. The optical density of Mn is too high to resolve the color band.
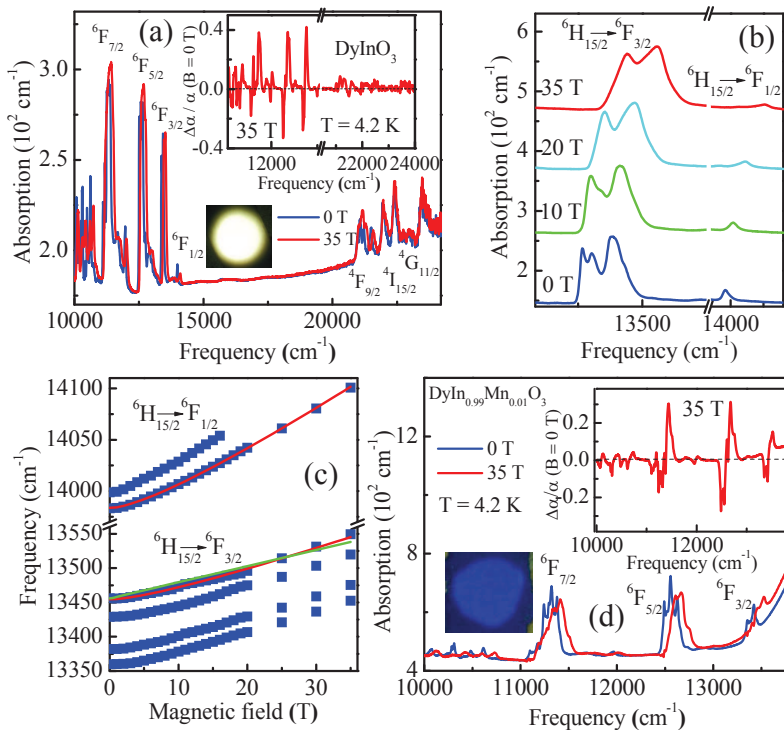
The two levels in this expression correspond to the ground and excited states of the rare-earth center. The relation fits the magnetization energy very well (for μ=8.1 μ_B), indicating that the peak position trends ($\approx$100 cm^{-1} at 35 T; 3 cm^{-1}/T) are dominated by ground state Zeeman effects. Taken together, our measurements reveal that magnetic field is quite effective at changing the position of the Dy^{3+} on-site excitations (3 cm^{-1}/T, 0.4 meV/T). By comparison, field-induced band gap shifts in conventional semiconductors due to Zeeman interactions are a similar order of magnitude (0.1 - 0.3 meV/T),[37,38] whereas those connected with magnetic phase transitions are much larger ($\geq$1.4 meV/T).[13,39]

The addition of Mn centers, for instance in $DyIn_{0.99}Mn_{0.01}O_3$, changes the color to a rich blue. This is due to the on-site excitations emanating from the Mn ions.[18] The effect on the magnetic properties is different. The paramagnetic impurities introduced by Mn substitution are located between the triangular layers. As a result, they act as free spins and have no effect on the behavior of the f-manifold crystal field excitations [Fig. 3(d)]. In fact, the field dependence of the f manifold excitations is the same as in the $DyInO_3$ parent compound and can be fit with exactly the same fitting parameters. This shows that addition of paramagnetic impurities has little effect on the localized f-manifold excitations.

III.4. Discussion of color change mechanisms

Materials that possess a large generalized susceptibility (i.e. a strong response to a small stimulus) are promising candidates for novel device applications. To that end, we have tested a number of different mechanisms, primarily but not exclusively in oxides. Collective transitions are among the most effective at amplifying spin-charge interactions and generating field-induced color changes because they modify local charge density distributions[13,21,40,41]. Examples include spin-flop and magnetic quantum critical transitions. $Ni_3V_2O_8$ is an especially interesting case because color contrast due to a field-tunable band edge can be seen with the naked eye. Color changes driven by magnetic field also occur in molecular systems due to a tunable singlet-triplet equilibrium and the differences in electronic structure between the two states.[29] Rare-earth excitations have many positive aspects in this regard including (i) strong intensities, (ii) excellent contrast, (iii) clear shifts with field due to Zeeman interactions, and (iv) resonances in the visible range - although f-manifold excitations also occur elsewhere. Moreover, spin-orbit coupling naturally mixes spin and charge. These excitations are, however, very sharp and their changes do not translate into substantial color contrast. A design strategy that places spin-orbit coupling on the five-fold coordinated trigonal-bipyramidal chromophore sites (currently occupied by Mn in the $RIn_{1-x}Mn_xO_3$ (R = Tb, Dy) system) is one path toward stronger interactions and broader spectral change. The development of Re analogs like $RIn_{1-x}Re_xO_3$ would be a straightforward next step. More generally, these data suggest that placing spin on heavy chromophores other than rare-earth centers is a promising variation. Systems containing 4 and 5d centers are examples of this more comprehensive design

strategy.[42]

IV. SUMMARY

We investigated the high field magnetic and optical properties of substituted rare-earth indium oxides with chemical formula RIn$_{1-x}$Mn$_x$O$_3$ (R = Tb, Dy). Applied field reveals saturating moments in these systems, a slightly higher magnetization due to the introduction of paramagnetic impurities, and a spin glass transition in the Dy compound. Moreover, short range spin-spin correlations preserve the characteristic shape of the magnetization well above the ordering temperature. Magnetic field also creates optical contrast. The edge states, on-site Mn^{3+} d to d excitations, and rare-earth f-manifold excitations all track the magnetization energy due to dominant Zeeman interactions. Spin-orbit coupling naturally mixes spin and charge, which is why field-induced modifications to the rare-earth excitations are so large. These data suggest that the next logical variation in the design strategy should be to bring spin-orbit coupling onto the trigonal bipyramidal chromophore site (for instance with a 4 or 5d center). Continued work in this direction will advance the understanding of spin-charge coupling away from the static limit.

V. ACKNOWLEDGEMENT

[1] K. Ishii, M. Fujita, T. Sasaki, M. Minola, G. Dellea, C. Mazzoli, K. Kummer, G. Ghiringhelli, L. Braicovich, T. Tohyama, K. Tsutsumi, K. Sato, R. Kajimoto, K. Ikeuchi, K. Yamada, M. Yoshida, M. Kurooka, and J. Mizuki, Nat. Comm. **5**, 3714, (2014).

[2] M. Fiebig, J. Phys. D: Appl. Phys. **38**, R123 (2005).

[3] K. F. Wang, J.-M. Liu, and Z. F. Ren, Adv. Phys. **58**, 321 (2009).

[4] Z. P. Yin, K. Haule, and G. Kotliar, Nat. Phys. **7**, 294 (2011).

[5] Y. S. Oh, S. Artyukhin, J. J. Yang, V. Zapf, J. W. Kim, D. H. Vanderbilt, and S. W. Cheong, Nature Comm. **5**, 3201 (2014).

[6] J. Ruiz-Fuertes , S. López-Moreno, J. López-Solano, D. Errandonea, A. Segura, R. Lacomba-Perales, A. Muñoz, S. Radescu, P. Rodríguez-Hernandez, M. Gospodinov, L. L. Nagornaya, and C. Y. Tu, Phys. Rev. B **86**, 125202 (2012).

[7] T. Goto, T. Kimura, G. Lawes, A. P. Ramirez, and Y. Tokura, Phys. Rev. Lett. **92**, 257201 (2004).

[8] T. Kimura, T. Goto, H. Shintanl, K. Ishzaka, T. Arima, and Y. Tokura, Nature **426**, 55 (2003).

[9] A. Asamitsu, Y. Moritomo, Y. Tomioka, T. Arima, and Y. Tokura, Nature (London) **373**, 407 (1995).

[10] H. Katsura, A. V. Balatsky, and N. Nagaosa, Phys. Rev. Lett. **98**, 027203 (2007).

[11] Ü. Özgür, Ya. I. Alivov, C. Liu, A. Teke, M. A. Reshchikov, S. Doğan, V. Avrutin, S.-J. Cho, and H. Morkoç, J. Appl. Phys. **98**, 041301 (2005).

[12] S. R. Basu, L. W. Martin, Y. H. Chu, M. Gajek, R. Ramesh, R. C. Rai, X. Xu, and J. L. Musfeldt, Appl. Phys. Lett. **92**, 091905 (2008).

[13] P. Chen, B. S. Holinsworth, K. R. O'Neal, T. V. Brinzari, D. Mazumdar, Y. Q. Wang, S. McGill, R. J. Cava, B. Lorenz, and J. L. Musfeldt, Phys. Rev. B **89**, 165120, (2014).

[14] B. Lorenz, ISRN Condensed Matter Physics **2013**, 497073, (2013).

[15] B. Van Aken, T. M. Palstra, A. Filippetti, and N. A. Spaldin, Nat. Mater. **3**, 164 (2004).

[16] W. T. Carnall, G. L. Goodman, K. Rajnak, and R. S. Rana, J. Chem. Phys. **90**, 3443 (1989).

[17] C. W. F. T. Pistorius and G. J. Kruger, J. Inorg, Nucl. Chem. **38**, 1471, (1976).

[18] A. E. Smith, H. Mizoguchi, K. Delaney, N. A. Spaldin, A. W. Sleight, M. A. Subramanian, J. Am. Chem. Soc. **131**, 17084 (2009).

[19] H. L. Yakel, W. C. Koehler, E. F. Bertant and E. F. Forrat, Acta Cryst. **16**, 957 (1963).

[20] The frustration parameter $f = |\theta_{CW}|/$T$_N$ in the hexa-RMnO$_3$ system ranges from 5.8 to 10.3.[43]

[21] W. S. Choi, S. J. Moon, S. S. A. Seo, D. Lee, J. H. Lee, P. Murugavel, T. W. Noh, and Y. S. Lee, Phys. Rev. B **78**, 054440 (2008).

[22] R. Cases, M. A. Chamarro, R. Alcala, and V. D. Rodriguez, J. Lumin. **49**, 509 (1991).

[23] P. A. Goddard, J. Singleton, P. Sengupta, R. D. McDonald, T. Lancaster, S. J. Blundell, F. L. Pratt, S. Cox, N. Harrison, J. L. Manson, H. I. Southerland, and J. A. Schlueter, New J. Phys. **10**, 083025 (2008).

[24] P. Chen, B. S. Holinsworth, K. R. O'Neal, N. Lee, C. V. Topping, S. McGill, S. -W. Cheong, J. Singleton, E. S. Choi, and J. L. Musfeldt, unpublished.

[25] J. L. Musfeldt, L. I. Vergara, T. V. Brinzari, C. Lee, L. C. Tung, J. Kang, Y. J. Wang, J. A. Schlueter, J. L. Manson, and M.-H. Whangbo, Phys. Rev. Lett. **103**, 157401 (2009).

[26] A. Walsh, J. L. F. Da Silva, S.-H. Wei, C. Korber, A. Klein, L. F. J. Piper, A. DeMasi, K. E. Smith, G. Panaccione, P. Torelli, D. J. Payne, A. Bourlange, and R. G. Egdell, Phys. Rev. Lett. **100**, 167402 (2008).

[27] F. Wooten, Optical properties of solids (New York, Academic Press, 1972).

[28] Error bars are large because of polycrystallinity and extrapolation from the edge of the absorption band.

[29] Ö. Günaydin-Sen, P. Chen, J. Fosso-Tande, T. L. Allen, J. Cherian, T. Tokumoto, P. M. Lahti, S. McGill, R. J. Harrison, and J. L. Musfeldt, J. Chem. Phys. **138**, 204716

(2013).

[30] N. W. Ashcroft, and N. D. Mermin, Solid state physics (Brooks Cole, 1976).

[31] P. Chen, Ö. Günaydın-Şen, W. J. Ren, Z. Qin, T. V. Brinzari, S. McGill, S. -W. Cheong, and J. L. Musfeldt, Phys. Rev. B **86**, 014407 (2012).

[32] P. Jiang, J. Li,, A. W. Sleight, and M. A. Subramanian, Inorg. Chem. **50** 5858 (2011).

[33] A. B. Souchkov, J. R. Simpson, M. Quijada, H. Ishibashi, N. Hur, J. S. Ahn, S. W. Cheong, A. J. Millis, and H. D. Drew, Phys. Rev. Lett. **91**, 027203 (2003).

[34] J. D. Axe and G. H. Dieke, J. Chem. Phys. **37**, 2364 (1962).

[35] M. Divis, J. Holsa, M. Lastusaari, A. P. Litvinchuk, and V. Nekvasil, J. Alloys Compd. **451**, 662 (2008).

[36] The zero field splitting energies are 13360, 13382, 13429, and 13456 cm^{-1} for the $^6H_{15/2} \rightarrow {}^6F_{3/2}$ excitation. The γ's are 13983 and 13999 cm^{-1} for the $^6H_{15/2} \rightarrow {}^6F_{1/2}$ excitation.

[37] K. Uchida, N. Miura, J. Kitamura, H. Kukimoto, Phys. Rev. B **53**, 4809 (1996).

[38] P. Bhattacharya, R. Fornari, and H. Kamimura, Comprehensive Semiconductor Science and Technology, Volume 2 (Elsevier Science, 2011).

[39] S. H. Jhang, M. Marganska, Y. Skourski, D. Preusche, M. Grifoni, J. Wosnitza, and C. Strunk, Phys. Rev. Lett. **106**, 096802 (2011).

[40] V. V. Eremenko, Yu. G. Litvinenko, and V. I. Myatlik, JETP Lett. **12**, 47 (1970).

[41] J. Cao, R. C. Rai, S. Brown, J. L. Musfeldt, R. Tackett, G. Lawes, Y. J. Wang, X. Wei, M. Apostu, R. Suryanarayanan, and A. Revcolevschi, Appl. Phys. Lett. **91**, 021913 (2007).

[42] B. J. Kim, H. Jin, S. J. Moon, J.Y. Kim, B. G. Park, C. S. Leem, J. Yu, T. W. Noh, C. Kim, S.-J. Oh, J.-H. Park, V. Durairaj, G. Cao, and E. Rotenberg, Phys. Rev. Lett. **101**, 076402 (2008).

[43] D. G. Tomuta, S. Ramakrishnan, G. J. Nieuwenhuys, and J. A. Mydosh, J. Phys.: Condens. Matter **13**, 4543 (2001).